ORIGINAL PAPER - CONDENSED MATTER

High-precision white light interferometry based on a color CCD and peak matching algorithm

Jaeseung Im[1] · Hyuntae Kim[1] · Woongkyu Park[2] · Jae Sung Ahn[3] · Byeongil Lee[4] · Soobong Choi[5]

Abstract

White light interferometry (WLI) is a widely used technique in various research fields because it can quickly measure the topography of a sample over a large area. In conventional WLI, the topography of the sample is generally obtained by using the envelope of the interferogram. However, this method cannot determine the precise order of the fringes because it is very sensitive to longitudinal chromatic aberration which may cause several measurement errors. Here, we propose an algorithm for avoiding errors in the measurement of the sample's topography. The concept of the peak matching algorithm and the development of a new scheme of acquiring the topography of the sample by using a color charge-coupled device (CCD) is proposed. We demonstrate that our method can reject the fringe distortion problem encountered when using a conventional WLI system to measure the discrete sample surface. We expect our method to be applied to a variety of research and in industrial fields that require precise topographic measurements.

Keywords White light interferometry · Color CCD camera · Peak matching algorithm · Topography

1 Introduction

In the semiconductor industry, high-resolution microscopy is essential to detect defects in devices or to evaluate their performances [1–4]. For these demands, high-resolution microscopies, such as electron beam microscopy, scanning

✉ Byeongil Lee
  bilee@pknu.ac.kr

✉ Soobong Choi
  sbchoi@inu.ac.kr

1 Department of Physics, Incheon National University, Academy-ro 119, Incheon 22012, Republic of Korea

2 Intelligent Sensor Convergence Research Center (ISCRC), Incheon National University, Academy-ro 119, Incheon 22012, Republic of Korea

3 Bio-Medical Photonics Research Center, Korea Photonics Technology Institute (KOPTI), Gwangju 61007, Republic of Korea

4 School of Information Technology and Convergence, Pukyong National University, Yongso-ro 45, Busan 48513, Republic of Korea

5 Department of Physics and Intelligent Sensor Convergence Research Center (ISCRC), Incheon National University, Academy-ro 119, Incheon 22012, Republic of Korea

probe microscopy, and phase-shifting interferometry (PSI), have been employed for various inspection processes [5–9]. Among them, PSI, which uses an optical interferometer, has received much attention because its measurement speed is faster than that of the others [10–15]. In conventional PSI systems, monochromatic lasers have been commonly used to measure the characteristics of the surfaces. Due to the use of a coherent light source, its height measurement range is limited to few times the wavelength when using phase unwrapping at smooth surface [14, 16]. Dual- and multi-wavelength phase-shifting interferometry and white light interferometry(WLI) have been introduced to overcome such limitations [17, 18]. Dual- or multi-wavelength phase-shifting interferometry uses a number of monochromatic waves to extend the unambiguous range [19]. Nevertheless, undesirable signals, such as speckles and multiple interference patterns, may still remain, which may reduce the usefulness of this technique.

WLI by using white light with a wide spectral range and short coherence length provides high height resolution, which make it a useful technique for measuring the topography of various devices with discontinuous heights [15, 20–22]. In conventional WLI, a monochromatic charged coupled device (CCD) was used to measure interferograms. However, when measuring the interferogram

and determining the zeroth-order fringe with a monochromatic CCD, several factors, such as the nonuniform spectrum of the light source and the absorption spectrum of the sample, may affect the results [23–27].

With the help of a color CCD, the combination of WLI and multi-wavelength techniques has been studied continuously because the advantage of using white light, for example, the high height resolution due to the low coherence and the ability to obtain interferograms of each color, can be utilized. For example, Upputuri et al. studied a fringe order determination method using the signal from each color channel and the Hilbert transform [28]. Tong Guo et al. studied a height measurement method using an evaluation function extracted from the phase value of each color channel [29]. Despite such efforts, a detector with limited pixel size would cause fringe distortion when measuring a discrete sample surface [29–32].

Here, we present a new data processing method for high-precision WLI based on a color CCD: the peak matching algorithm. Unlike the conventional analysis methods using the center wavelength of the full spectrum, our method analyzes the data by using the three center wavelengths of red, green, and blue light, respectively. The height resolution of WLI is improved by using the peak matching algorithm to analyze the interference patterns of each color. By comparing the WLI image with the atomic force microscopy image, we confirm that we can resolve the fringe distortion problem encountered when using conventional WLI.

2 Methods

2.1 WLI apparatus with a color CCD

We used an interferometric imaging system with a Mirau objective, as shown in Fig. 1a. A white light-emitting diode (PP00W-8L63-ESESBI, Photron Co., Ltd.) was used as an incoherent white light source. Samples with known geometries were placed on a z-axis piezo nano-positioning system (E-505.00 LVPZT Piezo Amplifier Module, Physik Instrumente (PI)). White light interference images generated by using × 10 Mirau objectives (Nikon) were obtained with a color CCD (Manta G-1236, Allied Vision). The pixel size of the CCD was 3.45 μm, and the total number of pixels was 4112 × 3008. In our experiments, the interference signals through $f = 180$ mm imaging lens were acquired only at 1028 × 752 pixels of the CCD for rapid data processing, as shown in Fig. 1b.

2.2 Image acquisition and processing

Interference images obtained with the color CCD were analyzed and processed by using the SciPy module in Python, as shown in Fig. 1c. Color images obtained with the CCD have red–green–blue (RGB) values for each pixel and scan position. We analyzed the RGB values of each pixel to obtain interferograms of each color. The interferogram of each color per pixel was processed by convolution with a one-dimensional Gaussian function (smoothing) and then

Fig. 1 Concept reported in this paper: **a** schematic of experimental setup, **b** interference fringes acquired by using three color CCD, and **c** flow of signal processing
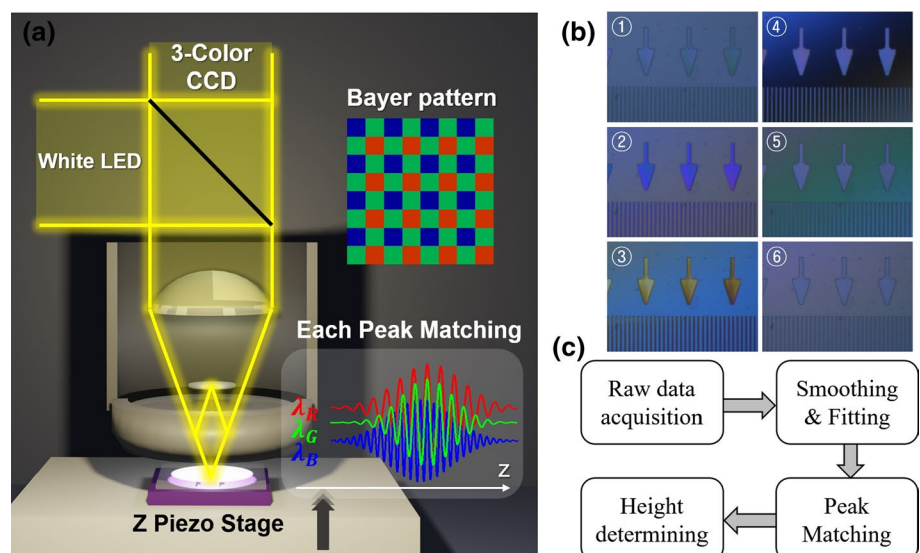
the interferogram was interpolated ten times. The smoothed and interpolated interferogram was fitted using an interference formula, which will be discussed in Sect. 2.3.

2.3 Peak matching algorithm

In an interferogram, the intensity of incoherent light with center wavelength λ_{cn} can be expressed as a function of displacement $z(x, y)$ as follows [13]:

$$
\begin{aligned}
I_n(x, y, z) = I_{0n} \\
+\gamma_n I_{0n} \exp\left(-\left(\frac{z(x, y) - z_{0n}}{l_{cn}}\right)^2\right) \cos\left(\frac{4\pi\left(z(x, y) - z_{0n}\right)}{\lambda_{cn}} + \phi(x, y)\right),
\end{aligned}
\tag{1}
$$

where I_{0n} is an offset of the intensity, γ_n is the visibility of the light, l_{cn} is the coherence length of the light, z_{0n} is a coherence peak position and ϕ is a phase difference between the light reflected from the sample surface and the reference mirror. We fitted the intensity interferogram of each color measured at each pixel by using Eq. (1). The range of the parameter z_{0n} is limited around the maximum peak position of the grayscale intensity interferogram. The fitted data were then divided into a certain period to obtain the local maximum point of each section, i.e., the point of the fringe center. The point with the strongest intensity of the envelope in the phase range of $[-\pi/2, \pi/2]$ was defined as the zeroth-order fringe [33–35].

The measured intensity can vary discontinuously due to various factors such as ambient vibrations. In addition,

scattered light from the edges of the structures or a nonuniform spectral density can affect the intensity measurements. In this case, the zeroth-order position obtained from the experimental measurements and fitting can be different. This discrepancy can result in a phase distortion in conventional WLI which uses the peak position of the envelope. Thus, though the local maximum point is not within the zeroth-order fringe, the point can represent the actual height of the sample. If the local maximum points that can be obtained from the RGB interferogram are represented as R_i, G_j, B_k (i, j, k = the order of the fringe), then the deviation function V_{ijk} can be defined as follows:

$$
V_{ijk} = \left|R_i - G_j\right| + \left|G_j - B_k\right| + \left|B_k - R_i\right|.
\tag{2}
$$

If the three points at which the deviation function V_{ijk} becomes minimum are defined as $R_{min}, G_{min}, B_{min}$, respectively, then we can define the average of those three points as the height of the sample.

$$
H = \frac{R_{min} + G_{min} + B_{min}}{3}.
\tag{3}
$$

Fig. 2 **a** Interferograms obtained from each color pixel. Interferograms convolved with one-dimensional Gaussian function (black dotted lines). Fitted interferograms obtained by using the Eq. (1) (color lines). **b** Fitted interferogram of each color obtained in (**a**) and the position of the fringes in each interferogram. **c** Concept of the peak matching algorithm
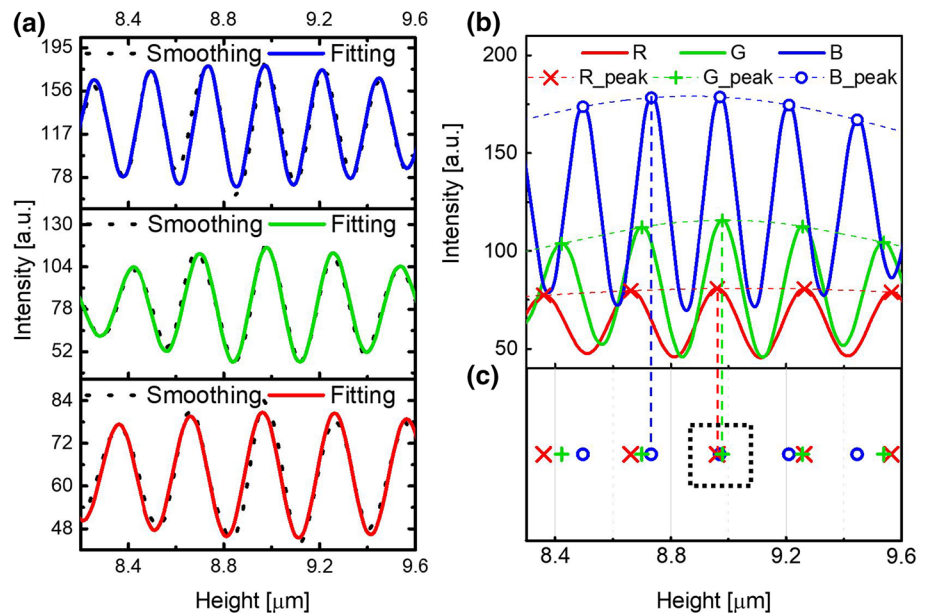
3 Results

The RGB interferograms at a certain pixel convolved with a one-dimensional Gaussian function are shown in Fig. 2a (black dotted lines). The corresponding fittings by using Eq. (1) are also shown in Fig. 2a (blue, green, and red lines in order from top to bottom). Each color response is well fitted at a non-zeroth-order fringe. The center wavelengths of each color are 596.5 nm, 548.6 nm, and 454.7 nm, respectively. Because the center wavelength of each color is different, the location of the local maximum points (i.e., the points at the center of each fringe) can be different. All fittings and local maximum points obtained from Fig. 2a are merged and shown in Fig. 2b.

In the R and G interferograms, the zeroth-order fringes are located at 8.962 and 8.980 μm, respectively. On the other hand, in the B interferogram, the zeroth-order fringe is located at 8.732 μm and is somewhat different from the values of R and G. In B, the first order fringe is located at a point similar to the zeroth-order fringe of R and G. Figure 2c shows the peak positions of all fringes in the interferograms shown in Fig. 2b. The three dots in the black dotted square represent the points that are each in a different order, but minimize the deviation function V_{ijk}. Therefore, those points become $R_{min}, G_{min}, B_{min}$, respectively, and the height of the sample at a certain pixel can be obtained by calculating the position average of these three points.

Topographic images and line profiles obtained by using interferograms of each color and the peak matching algorithm are shown in Fig. 3. Figure 3a–c shows the mappings of $R_{min}, G_{min}, B_{min}$, respectively. The cross-sectional profiles of lines 1 and 2 in each image are also shown in Fig. 3d–f. All measured step heights on lines 1 and 2 are approximately 1.75 μm.

Figure 4 shows a comparison of topographic images taken by using contact mode atomic force microscopy (C-AFM, NX-12, Park Systems Corp.) with those obtained using WLI with the peak matching algorithm. Figure 4d shows the cross-sectional profile of the area indicated by the dashed white line (denoted by A' and B') in Fig. 4a. The measured step heights in A' and B' are 1.747 and 1.751 μm, respectively. When WLI is used, the step heights were measured to be 1.750 and 1.752 μm, respectively (lines 1 and 2 in Fig. 4b, e), which are in good agreement with those measured by using C-AFM. The magnified interferogram of B (blue) is shown in Fig. 4c. The star and the black and the blue arrows represent the peak position of the envelope and the measured and corrected zeroth-order position, respectively. The positions indicated by each symbol were 8.856, 8.734, and 8.970 μm, respectively. We compared line profiles obtained by the conventional method using the peak position of the envelope those obtained by using the proposed peak matching algorithm in Fig. 4f. In contrast to the step height obtained with the conventional WLI system, the step height obtained with our WLI system can be seen to match clearly the original step height measured by using C-AFM.
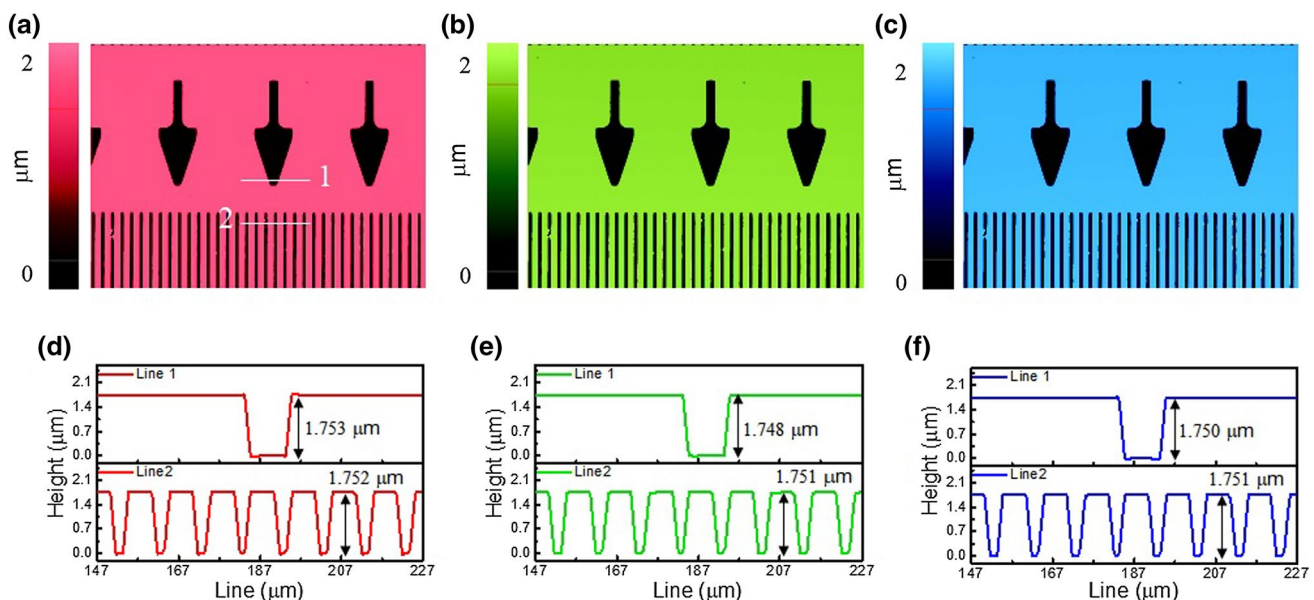

Fig. 3 **a–c** Topography of WLI images obtained for each color: **a** red, **b** green and **c** blue peaks. **d–f** Cross-sectioned line profiles of (**a**), (**b**) and (**c**) at lines 1, 2, respectively
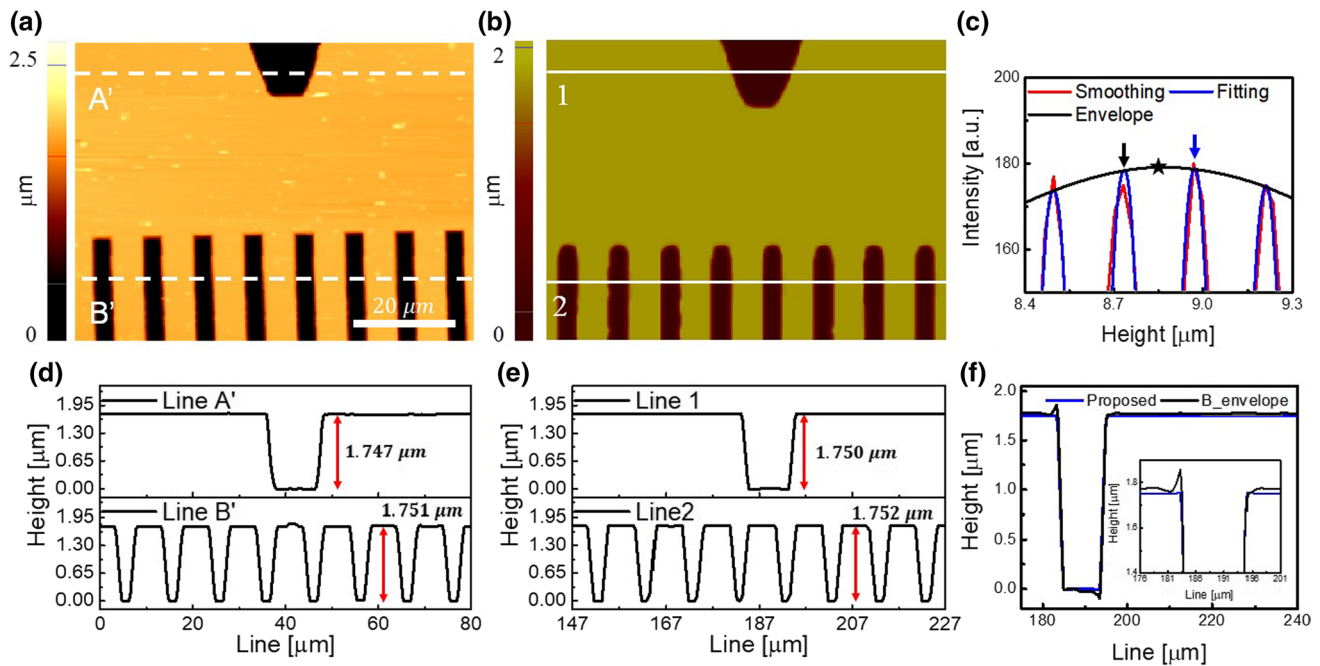
Fig. 4 a Topography image of the sample surface obtained by atomic force microscopy and **b** by 3-color WLI. **c** Interference responses of blue channel around peak position. **d**, **e** Line profiles of (**a**) and (**b**), respectively. **f** The profiles of line 1 obtained by using peak matching algorithm (blue solid line) and envelope maximum position of blue channel (black solid line)

4 Discussion

As mentioned in the Methods, we used the fitted data instead of the smoothed data. This is because the measured data are discontinuous; therefore, the peak positions may vary. Because the responsivity of the color CCD and the intensity of the white light are functions of wavelength, the measured RGB interferogram shown in Fig. 2a can be different from the fitted one. In addition, the existence of structures with two different heights in the same field of view can cause distortion of the interferogram due to scattering effects, which also results in a discrepancy between the measured and the fitted data [29, 31, 32]. Nevertheless, the phase near the zeroth-order fringe of the fitted data should be the same as the phase of the measured data. Therefore, one of the local maximum points should correspond to the point where the optical path difference becomes zero. One of the characteristics of the Mirau interferometry is that the light is focused on the point where the optical path difference is zero. If two structures with a large height difference are in the same field of view, the focal point may be formed only on one structure and not on the other. Then, the light at a point that is out of focus can affect other points that are in focus. Therefore, for each pixel, one should fit the data within the coherence length. The measured zeroth-order point (i.e., the point at which the intensity becomes maximum) may not actually be the one. The peak matching algorithm determines the

actual zeroth-order point of each interferogram by finding the minimum deviation of these points. Although a phase difference between the reference mirror and the sample exists, the peaks taken from responses obtained by using three different wavelengths are complementary.

In Fig. 3a–c, topographic images obtained using R_{min}, G_{min}, and B_{min} are shown. Although each topography was in good agreement with the topography obtained by using C-AFM, the R_{min}, G_{min}, and B_{min} values were averaged to further reduce unexpected noise.

For a comparison of the topographies obtained from our WLI system and from the conventional one, the cross-sectional profiles obtained by each method were plotted as shown in Fig. 4f. As mentioned in "Results", the position of the zeroth-order fringe can be different for each color. This difference can affect the position of the envelope peak, which results in the fringe distortion problem. Therefore, when the topography was measured with the conventional WLI, the depth of the trench became deeper and the height of the top layer became higher than that measured with C-AFM. That is, the step height discrepancy obtained with C-AFM and the conventional WLI is mainly due to the difference in the position of the zeroth-order fringe in the RGB interferogram. This uncertainty arises when the height difference is less than a quarter of the central wavelength of the white light. That is, an error of $\pm\lambda/2$ may occur in the step height of the sample. With the color CCD and the peak matching algorithm, we were able to prevent the fringe

distortion problem by finding the local maximum points of the interferograms where the deviation function became minimum. Furthermore, the batwing effect at the edge of the structure in the cross-sectional profile obtained by using the conventional WLI can also be dealt with by using the proposed peak matching algorithm (Fig. 4f). The batwing effect is resulted in combination of interference signal and scattering signal at the edge. Because scattering intensity is strongly related with a wavelength, separated RGB interference signal analysis can powerful key in this regime.

Although various studies have been done using color CCD in the WLI system, our research shows the first result that resolves the fringe distortion problem by using the color CCD-based WLI system and the peak matching algorithm. Therefore, our results will provide insights into various research fields that require precise topographic measurements.

5 Conclusion

We demonstrated that better height resolution can be achieved by using a color CCD-based WLI system and the peak matching algorithm rather than by using the conventional WLI system. The peak matching algorithm, which uses the local maximum points of the three interferograms and the deviation function, is able to reduce the uncertainty of the height compared to the conventional method, which uses the peak position of the envelope. As a result, we have successfully resolved the fringe distortion problem encountered when using the conventional WLI system. The topography measured with our method is consistent with the original sample structure. We believe that the results hold great potential for use in various research and industrial fields, such as device physics or biology, where precise topographic measurements are required.

References

1. C. Edwards, A. Arbabi, G. Popescu, L.L. Goddard, Optically monitoring and controlling nanoscale topography during semiconductor etching. Light Sci. Appl. **1**, e30–e30 (2012)
2. H.-S. Jang, T.H. Kim, T.H. Kim, J.S. Lee, J.H. Sin, B.H. Kim, Effect of high H_2 pressure on the structural and the electrical properties of MoS_2. J. Korean Phys. Soc. **79**, 38–43 (2021). https://doi.org/10.1007/s40042-021-00181-4
3. X. Jiang, N. Senin, P.J. Scott, F. Blateyron, Feature-based characterisation of surface topography and its application. CIRP Ann. **70**(2), 681–702 (2021). https://doi.org/10.1016/j.cirp.2021.05.001
4. D. Cooper, T. Denneulin, N. Bernier, A. Béché, J.-L. Rouvière, Strain mapping of semiconductor specimens with nm-scale resolution in a transmission electron microscope. Micron **80**, 145–165 (2016)
5. J. Kang, C. Hong, Resolution of closely-positioned optical vortices by phase-shifting interferometry. J. Korean Phys. Soc. **53**, 3827–3831 (2008)
6. F.J. Giessibl, Advances in atomic force microscopy. Rev. Mod. Phys. **75**, 949 (2003)
7. P. Hariharan, B.F. Oreb, T. Eiju, Digital phase-shifting interferometry: a simple error-compensating phase calculation algorithm. Appl. Opt. **26**, 2504–2506 (1987)
8. N. Feltin, S. Ducourtieux, L. Crouzier, A. Delvallée, K. Dirscherl, G. Zeng, in *Scanning probe microscopy (SPM)*, Charact. Nanoparticles (Elsevier, 2020), pp. 49–63
9. K.C.A. Smith, C.W. Oatley, The scanning electron microscope and its fields of application. Br. J. Appl. Phys. **6**, 391 (1955)
10. K. Creath, in *V phase-measurement interferometry techniques*, Prog. Opt. (Elsevier, 1988) pp. 349–393
11. Y.-D. Su, S.-J. Chen, T.-L. Yeh, Common-path phase-shift interferometry surface plasmon resonance imaging system. Opt. Lett. **30**, 1488–1490 (2005)
12. X. Su, W. Chen, Reliability-guided phase unwrapping algorithm: a review. Opt. Lasers Eng. **42**, 245–261 (2004)
13. P.J. de Groot, *Handbook of Optical Metrology: Principles and Applications*, 2nd edn, vol. 1. (CRC Press, Boca Raton, 2015), pp. 791–828
14. Z. Malacara, M. Servin, *Interferogram analysis for optical testing*, 2nd edn (CRC Press, Boca Raton, 2018)
15. P. Hariharan, *Basics of interferometry*, 2nd edn (Elsevier, Amsterdam, 2010)
16. P. de Groot, Principles of interference microscopy for the measurement of surface topography. Adv. Opt. Photon. **7**, 1–65 (2015)
17. Y.-Y. Cheng, J.C. Wyant, Two-wavelength phase shifting interferometry. Appl. Opt. **23**, 4539–4543 (1984). https://doi.org/10.1364/AO.23.004539
18. Y.-Y. Cheng, J.C. Wyant, Multiple-wavelength phase-shifting interferometry. Appl. Opt. **24**, 804–807 (1985). https://doi.org/10.1364/AO.24.000804
19. P.K. Upputuri, M. Pramanik, K.M. Nandigana, M.P. Kothiyal, Multi-colour microscopic interferometry for optical metrology and imaging applications. Opt. Lasers Eng. **84**, 10–25 (2016)
20. G.S. Kino, S.S.C. Chim, Mirau correlation microscope. Appl. Opt. **29**, 3775–3783 (1990)
21. S. Yang, G. Zhang, A review of interferometry for geometric measurement. Meas. Sci. Technol. **29**, 102001 (2018)
22. J.C. Wyant, in *White light interferometry*, Proc. SPIE (2002). https://doi.org/10.1117/12.474947
23. S. Wang, T. Liu, J. Jiang, K. Liu, J. Yin, Z. Qin, S. Zou, Zero-fringe demodulation method based on location-dependent birefringence dispersion in polarized low-coherence interferometry. Opt. Lett. **39**, 1827–1830 (2014)
24. A. Harasaki, J.C. Wyant, Fringe modulation skewing effect in white-light vertical scanning interferometry. Appl. Opt. **39**, 2101–2106 (2000)
25. P. Lehmann, P. Kühnhold, W. Xie, Reduction of chromatic aberration influences in vertical scanning white-light interferometry. Meas. Sci. Technol. **25**, 65203 (2014). https://doi.org/10.1088/0957-0233/25/6/065203
26. L. Zhu, Y. Dong, Z. Li, X. Zhang, A novel surface recovery algorithm for dual wavelength white LED in vertical scanning interferometry (VSI). Sensors **20**, 5225 (2020)
27. S. Wang, T. Liu, J. Jiang, K. Liu, J. Yin, F. Wu, Birefringence dispersion compensation demodulation algorithm for polarized low-coherence interferometry. Opt. Lett. **38**, 3169–3172 (2013)
28. P.K. Upputuri, L. Gong, H. Wang, M. Pramanik, K.M. Nandigana, M.P. Kothiyal, Measurement of large discontinuities using single white light interferogram. Opt. Express. **22**, 27373–27380 (2014)

29. T. Guo, Y. Gu, J. Chen, X. Fu, X. Hu, in *Surface topography measurement based on color images processing in white light interferometry*, Opt. Meas. Syst. Ind. Insp. IX, International Society for Optics and Photonics (2015), p. 952511

30. Y. Sun, H. Yu, J. Ma, Q. Hu, X. Huang, J. Zhou, P. Xie, Z. Yang, L. Lei, Y. Fu, Spurious fringe processing for dielectric metasurface profile measurement using white-light scanning interferometry. Appl. Opt. **60**, 215–223 (2021)

31. J. Niehues, P. Lehmann, in *Improvement of lateral resolution and reduction of batwings in vertical scanning white-light interferometry*, Opt. Meas. Syst. Ind. Insp. VII, International Society for Optics and Photonics (2011), p. 80820W

32. T. Guo, F. Li, J. Chen, X. Fu, X. Hu, Multi-wavelength phase-shifting interferometry for micro-structures measurement based on color image processing in white light interference. Opt. Lasers Eng. **82**, 41–47 (2016)

33. Q. Vo, F. Fang, X. Zhang, H. Gao, Surface recovery algorithm in white light interferometry based on combined white light phase shifting and fast Fourier transform algorithms. Appl. Opt. **56**, 8174–8185 (2017)

34. S. Kim, J. Kim, H. Pahk, Fringe-order determination method in white-light phase-shifting interferometry for the compensation of the phase delay and the suppression of excessive phase unwrapping. J. Opt. Soc. Korea. **17**, 415–422 (2013)

35. Y.S. Ghim, A. Davies, Complete fringe order determination in scanning white-light interferometry using a Fourier-based technique. Appl. Opt. **51**, 1922–1928 (2012). https://doi.org/10.1364/AO.51.001922

Publisher's Note Springer Nature remains neutral with regard to jurisdictional claims in published maps and institutional affiliations.